Plasmonic Hot-Electron-Assisted Ultra-Stretchable Hydrogel Electrodes for Wearable Cardiovascular Monitoring and AI-Driven Predictive Analytics

Bangul Khan[1,2], Syed Bilal Ahmed[3], Bilawal Khan[4], Muhammad Shehzad[2], Liangyi Lyu[2,5] Iyapan Gunasekran[2], Raffi u Shan Ahmad[1,2], Junchen Liao[1], Mohammad El Hosseini[1]*, Bee Luan KHOO[1,2,6]*

[1]Department of Biomedical Engineering, College of Biomedicine, City University of Hong Kong, Tat Chee Ave, Kowloon, Hong Kong SAR.

[2]Hongkong Center of Cerebro-Cardiovascular Health Engineering (COCHE), Shatin, Hong Kong.

[3]School of Science, Herbin Institute of Technology (Shenzhen), Shenzhen 518055, China.

[4]Department of Material Science and Engineering, City University of Hong Kong, Tat Chee Ave, Kowloon, Hong Kong SAR.

[5]Department of Electrical Engineering, City University of Hong Kong, Tat Chee Ave, Kowloon, Hong Kong SAR.

[6]City University of Hong Kong – Futian Shenzhen Research Institute.

*Correspondence: Bee Luan Khoo, blkhoo@cityu.edu.hk, Mohamed Elhousseini Hilal, melhouss@um.city.edu.hk

Supporting Table 1: Detailed Formulation of the samples

S: No	AM	PEDOT: PSS	Ag-NPs	H_2O	Glycerol	MBAA	APS
S1	3.6g	-	-	8ml	2ml	0.009g	0.09g
S2	3.6g	50ul	-	8ml	2ml	0.009g	0.09g
S3	3.6g	100ul	-	8ml	2ml	0.009g	0.09g
S4	3.6g	300ul		8ml	2ml	0.009g	0.09g
S5	3.6g	100ul	5mg	8ml	2ml	0.009g	0.09g
S6	3.6g	100ul	10mg	8ml	2ml	0.009g	0.09g
S7	3.6g	100ul	20mg	8ml	2ml	0.009g	0.09g

AM: Acrylamide, APS: Ammonium persulfate, MBA: N, N'-methylene bisacrylamide

Supporting Table 2: Detailed Formulation of the subjects

Subject Number	Gender	Age	Height (cm)	Medical History
S1	Male	32 years	170	Healthy
S2	Male	36 years	172	Healthy
S3	Male	32 years	172	Asthma
S4	Male	26 years	173	Healthy
S5	Male	29 years	180	Healthy
S6	Male	32 years	179	Healthy
S7	Male	36 years	168	Healthy
S8	Male	49 years	164	Healthy
S9	Male	26 years	189	Healthy
S10	Female	29 years	153	Healthy
S11	Female	22 years	158	Healthy
S12	Female	32 years	160	Healthy
S13	Female	26 years	150	Healthy
S14	Female	23 years	160	Healthy
S15	Female	26 years	150	Healthy
S16	Female	25 years	160	Healthy
S17	Female	22 years	160	Healthy
S18	Male	25 years	165	Healthy
S19	Male	31 years	160	Healthy
S20	Male	27 years	167	Healthy

Supporting Table 3: State of the Art comparison with the reported literature

S: No	Materials	Stretchability	Geleation time	Biocompatibility	Self-Adhesiveness	Antibacterial	AI integration	References
1	Rotaxane hydrogels (PR-Gel)	830	60 minutes	NA	Yes	NA	NA	[1]
2	Ag–LM–PVA organogel	400	15 min	NA	NA	NA	NA	[2]
3	PVA-PEDOT:PSS	962	10 minutes	NA	NA	NA	NA	[3]
4	MXene-PAA-ACC hydrogel	450	2 minutes	Yes	NA	NA	NA	[4]
5	PAACP conductive hydrogel	1000	120 minutes	Yes	Yes	NA	NA	[5]
6	HPM-Y	1950	120 minutes	Yes	Yes	Yes	NA	[6]
7	Ag-LPA hydrogel	1072	5 minutes	Yes	Yes	Yes	NA	[7]

8	PAM-1%PEDOT:PSS-10% Ag	2200	7 minutes	Yes	Yes	Yes	Yes	This Work

Supporting Table 4: Radar chart comparing data of multifunctional performance, including key parameters: stretchability, conductivity, antibacterial activity, biocompatibility, and AI integration.

Hydrogel	Stretchability	Conductivity	Antibacterial	Biocompatibility	AI integration	Reference
ILn@MXene multifunctional hydrogel	1903	1.48	Yes	Yes	NA	[8]
PEDOT:PSS@HEC/PAM dual-network hydrogel	1060	0.42	NA	NA	NA	[9]
PAM–PEDOT:PSS hydrogel	646	2.5	NA	Yes	NA	[10]
PAM/SS/PEDOT: PSS	2120	0.45	NA	NA	NA	[11]
PPMP-OH organohydrogel	772	0.25	NA	NA	NA	[12]
PAAM-SA-MXene-PEDOT: PSS Composite Hydrogel	1350	1.6	NA	NA	Yes	[13]
PU@MXene/PAM Hydrogel	1834	0.05	NA	NA	NA	[14]
PAM/HPMC/PEDOT: PSS hydrogel	1600	0.25	NA	NA	NA	[15]
PAA/SCMC/$Ti_3C_2T_X$/Sn^{4+} hydrogel	1688	0.82	NA	NA	NA	[16]
PVA/MXene /Zn2+/Gly	250	0.056	Yes	NA	NA	[17]
PVA/PAM/ MXene/EG	1000	0.02	NA	NA	NA	[18]
PAM/TA@C	1500	0.11	NA	NA	NA	[19]

NF/MXene/ Gly						
PAM/PAA/ CS/MXene/ Gly	918	1.34	NA	NA	NA	[20]
PAM-PEDOT: PSS-Ag NPs	2200	0.33	Yes	Yes	Yes	This work

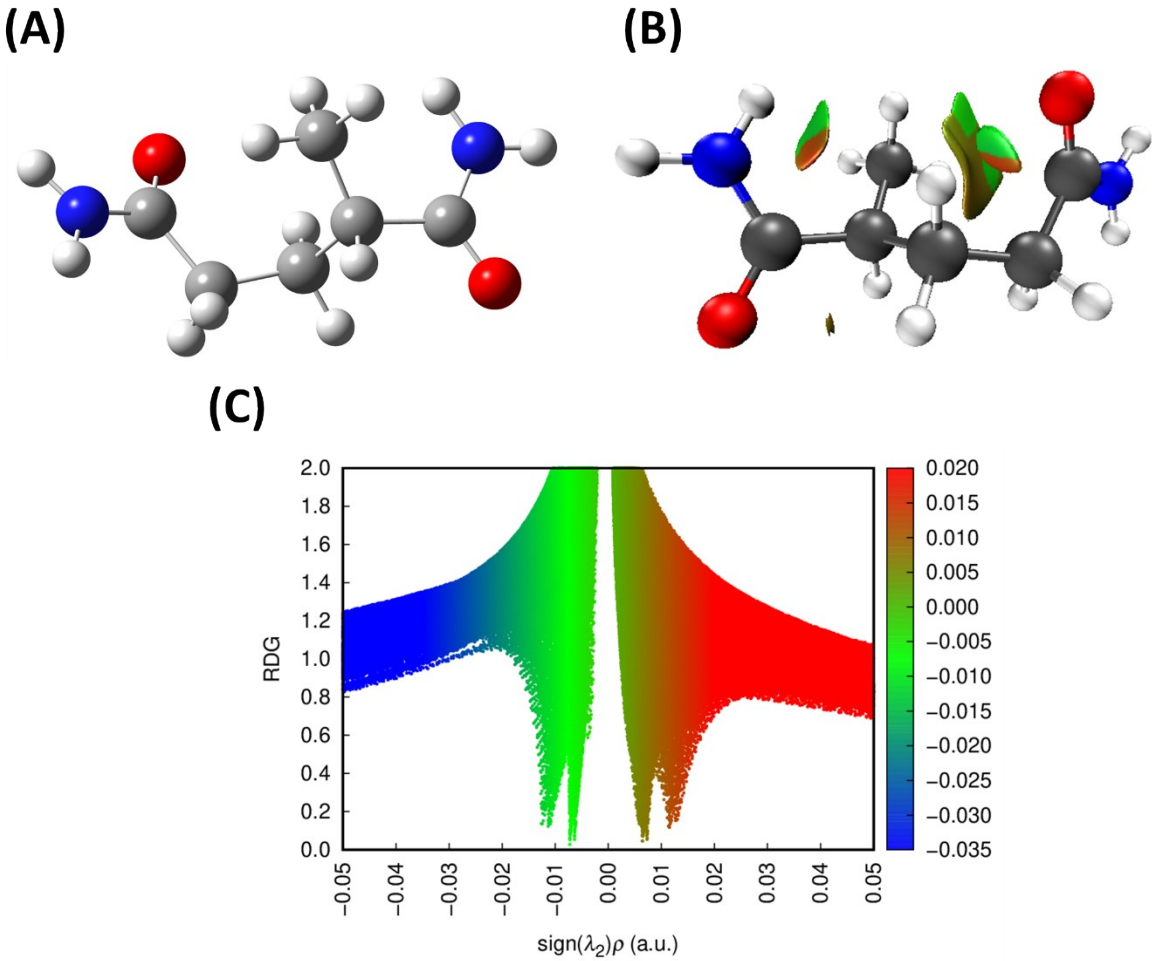

Supporting Figure 1. Non-Covalent Interaction Analysis of PAM. (A) Optimised molecular structure of PAM, (B) NCI Simulated molecular structure of PAM, (C) RDG Plot of PAM.

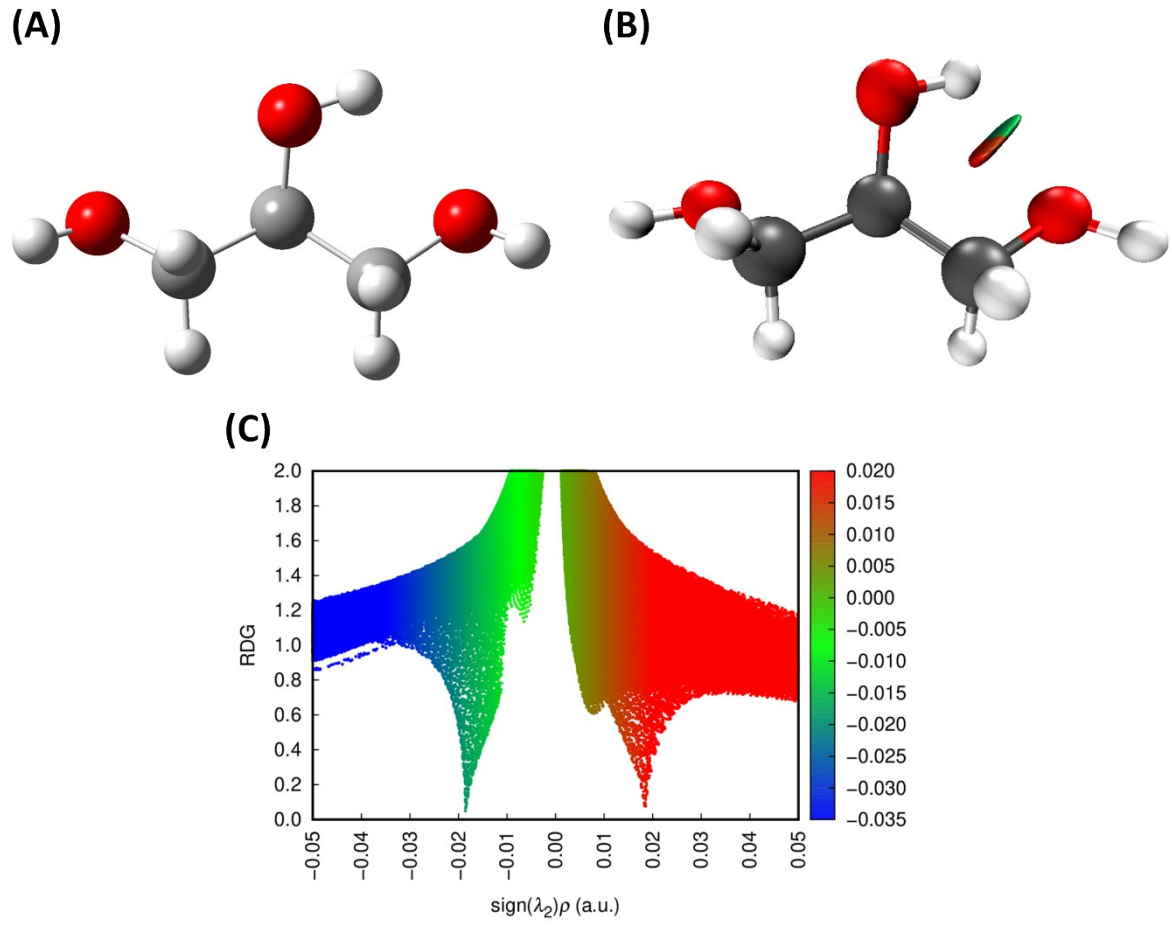

Supporting Figure 2. Non-Covalent Interaction Analysis of Glycerol. (A) Optimised molecular structure of Glycerol, (B) NCI Simulated molecular structure of Glycerol, (C) RDG Plot of Glycerol.

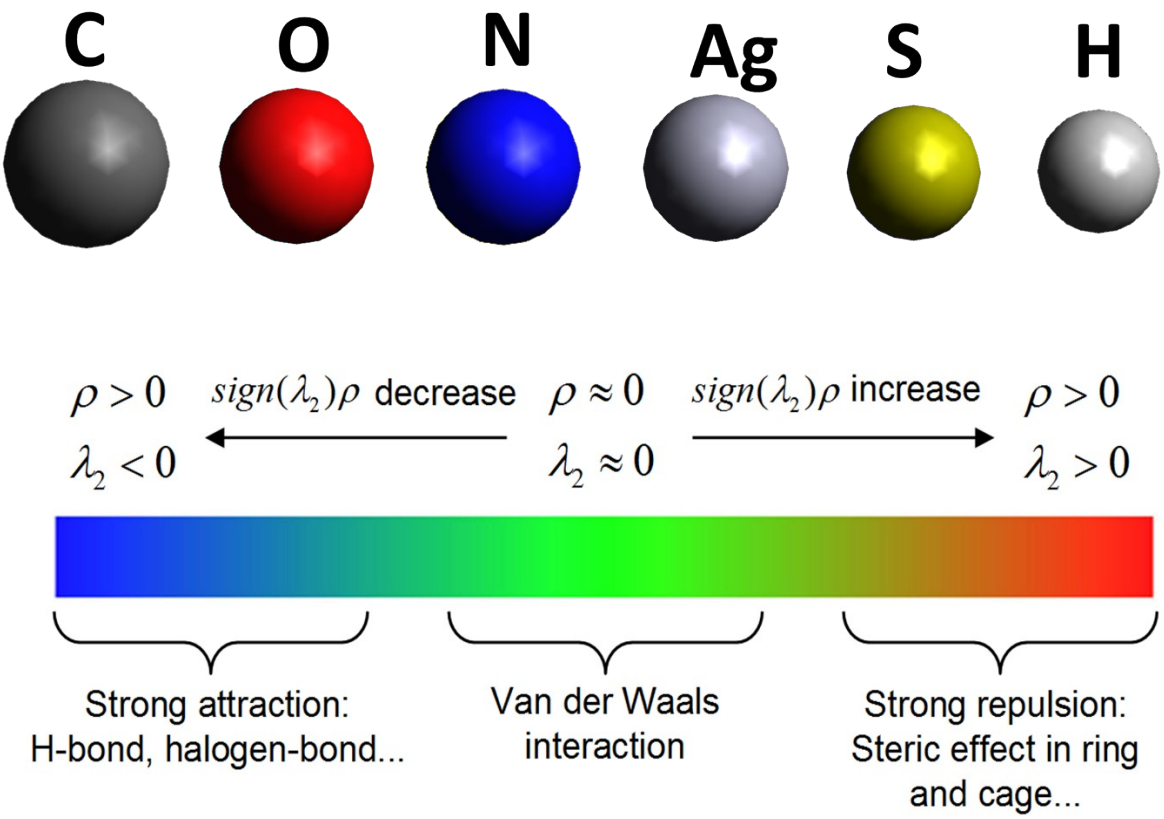

Supporting Figure 3. Colour codes of elements used in NCI analysis and the RDG plots reference colour bar.

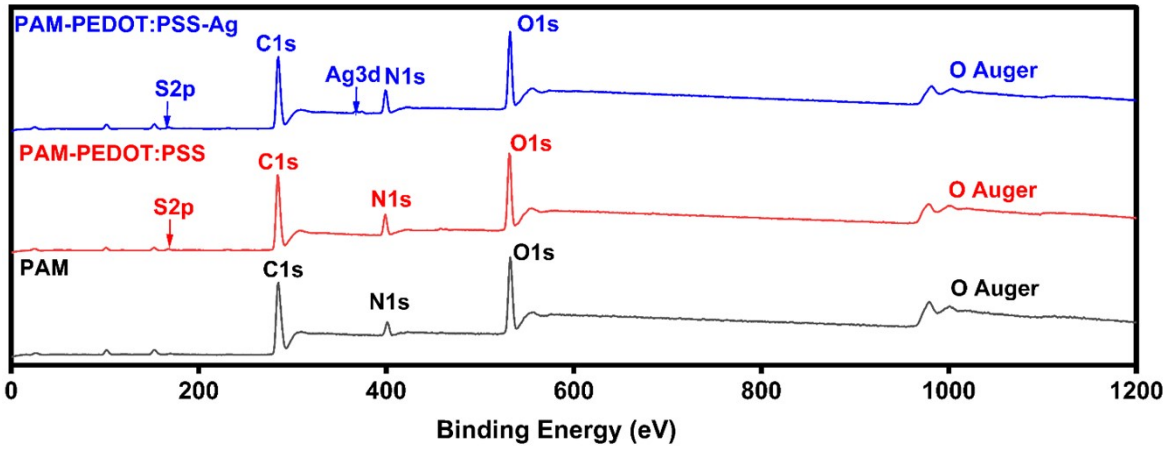

Supporting Figure 4. XPS Survey of PAM, PAM- 1% PEDOT: PSS, PAM- 1%PEDOT: PSS- 10% Ag

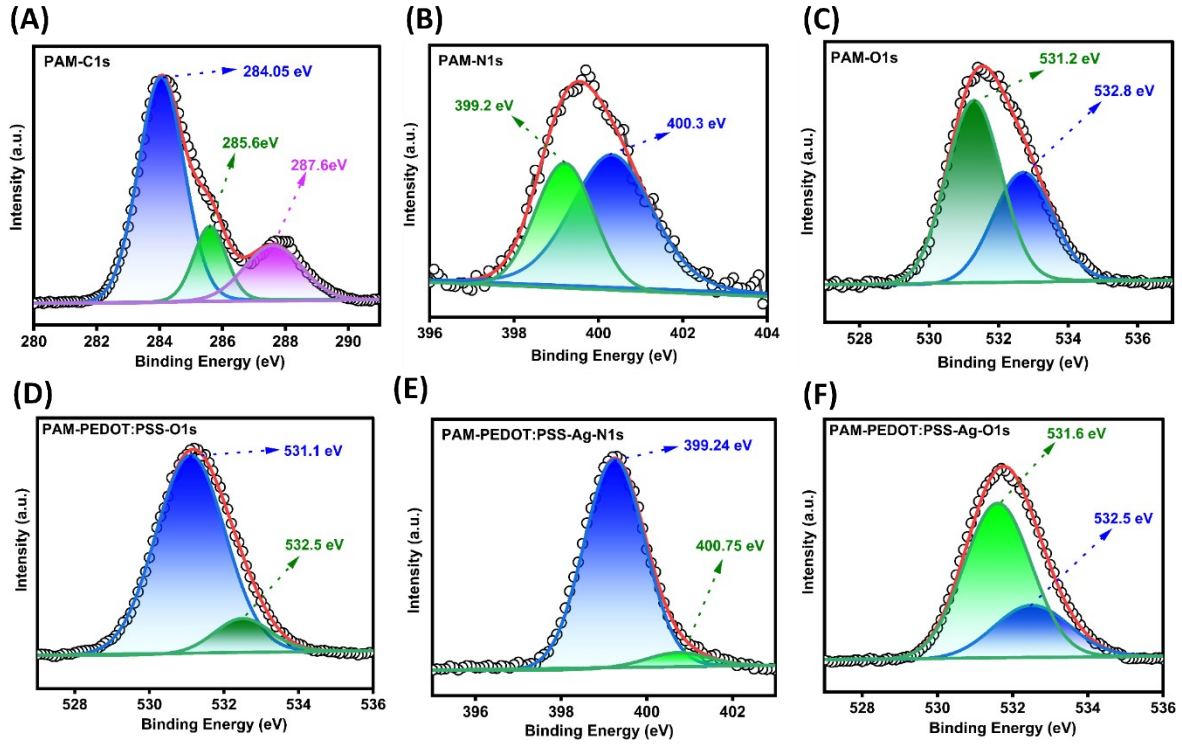

Supporting Figure 5. XPS deconvoluted peaks of PAM, PAM- 1% PEDOT: PSS, PAM-1% PEDOT: PSS-10% Ag, A. XPS deconvolution of the C1s peak of PAM, B. XPS deconvolution of the N1s peak of PAM, C. XPS deconvolution of the O1s peak of PAM, D. XPS deconvolution of the O1s peak of PAM- 1% PEDOT: PSS, E. XPS deconvolution of the N1s peak of PAM- 1% PEDOT: PSS- 10% Ag, F. XPS deconvolution of the O1s peak of PAM-1% PEDOT: PSS- 10% Ag.

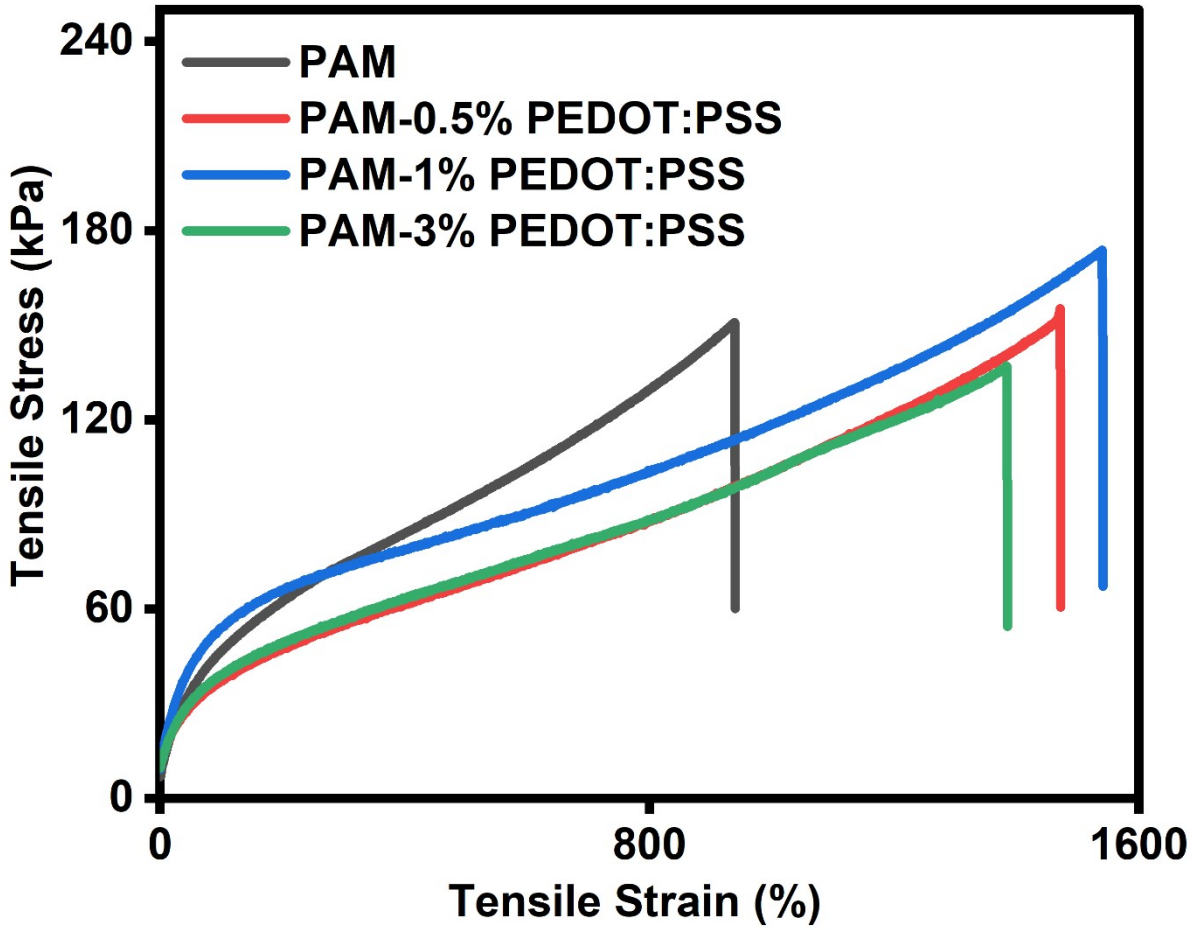

Supporting Figure 6. Stress-strain curves for PAM, PAM-0.5% PEDOT: PSS, PAM-1% PEDOT: PSS, PAM- 3% PEDOT: PSS hydrogels

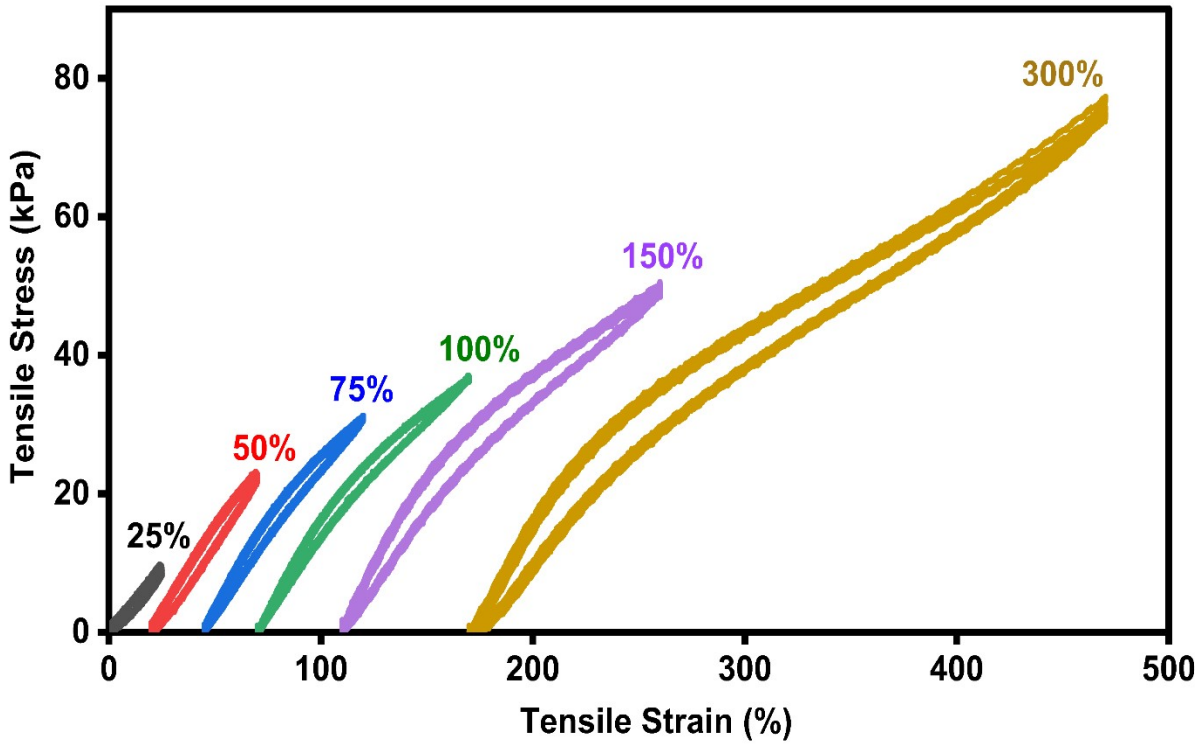

Supporting Figure 7. Cyclic stress-strain curves of PAM-1% PEDOT: PSS-10% Ag hydrogels at strains of 25%, 50%, 75%, 100%, 150%, and 300%.

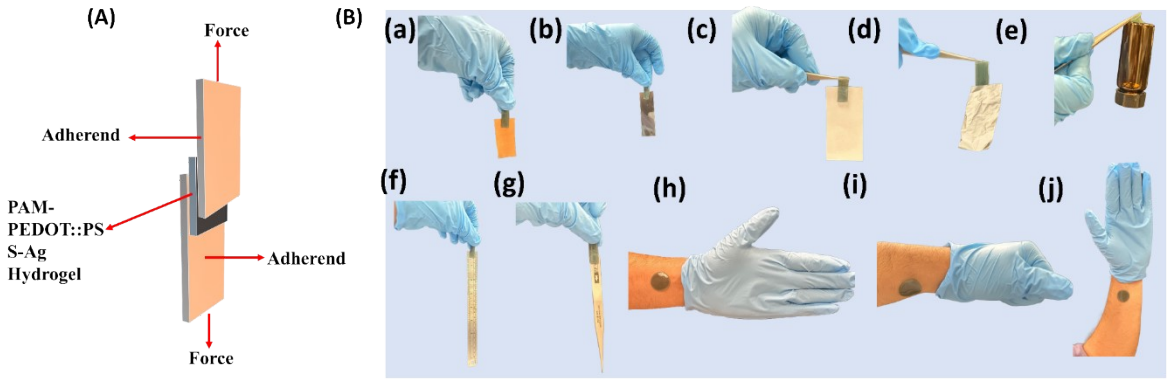

Supporting Figure 8. Adhesion testing of PAM- 1% PEDOT: PSS-10% Ag. (A) Visual demonstration of a lap-shear test for analysing adhesion properties of PAM-PEDOT: PSS-10% Ag, (B) Visually illustration of the PAM- 1% PEDOT: PSS-10% Ag hydrogel's adhesion to diverse surfaces, including copper (a), iron (b), tissue paper (c), aluminium (d), glass (e), a foot scale (f), tweezers (g), and the human hand at various angles (h-j).

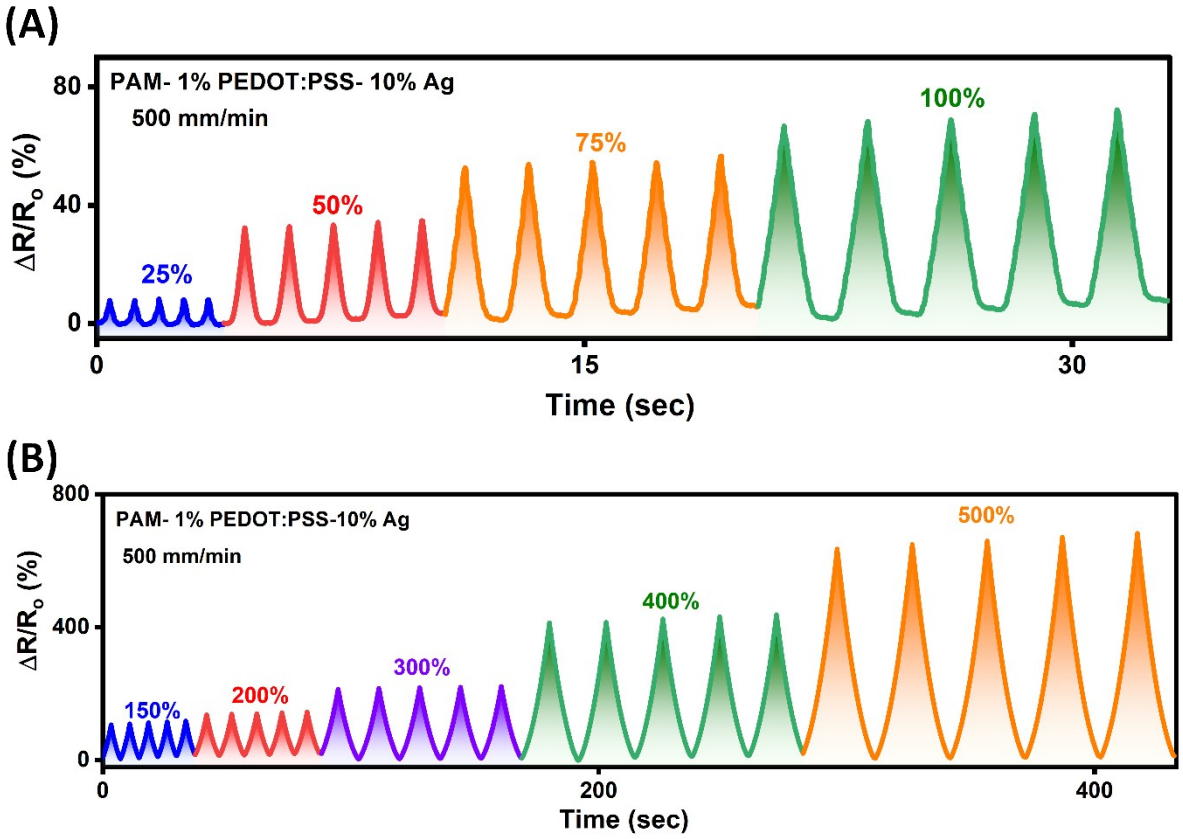

Supporting Figure 9. Strain testing of PAM- 1% PEDOT: PSS-10% Ag hydrogel (A) Relative resistance changes ($\Delta R/R_o$ %) in PAM- 1% PEDOT: PSS-10% Ag hydrogel over a 25%-100% at a 500 mm/min rate. (B) Relative resistance changes ($\Delta R/R_o$ %) in PAM- 1% PEDOT: PSS-10% Ag hydrogel over a 150% 500% at a 500 mm/min rate.

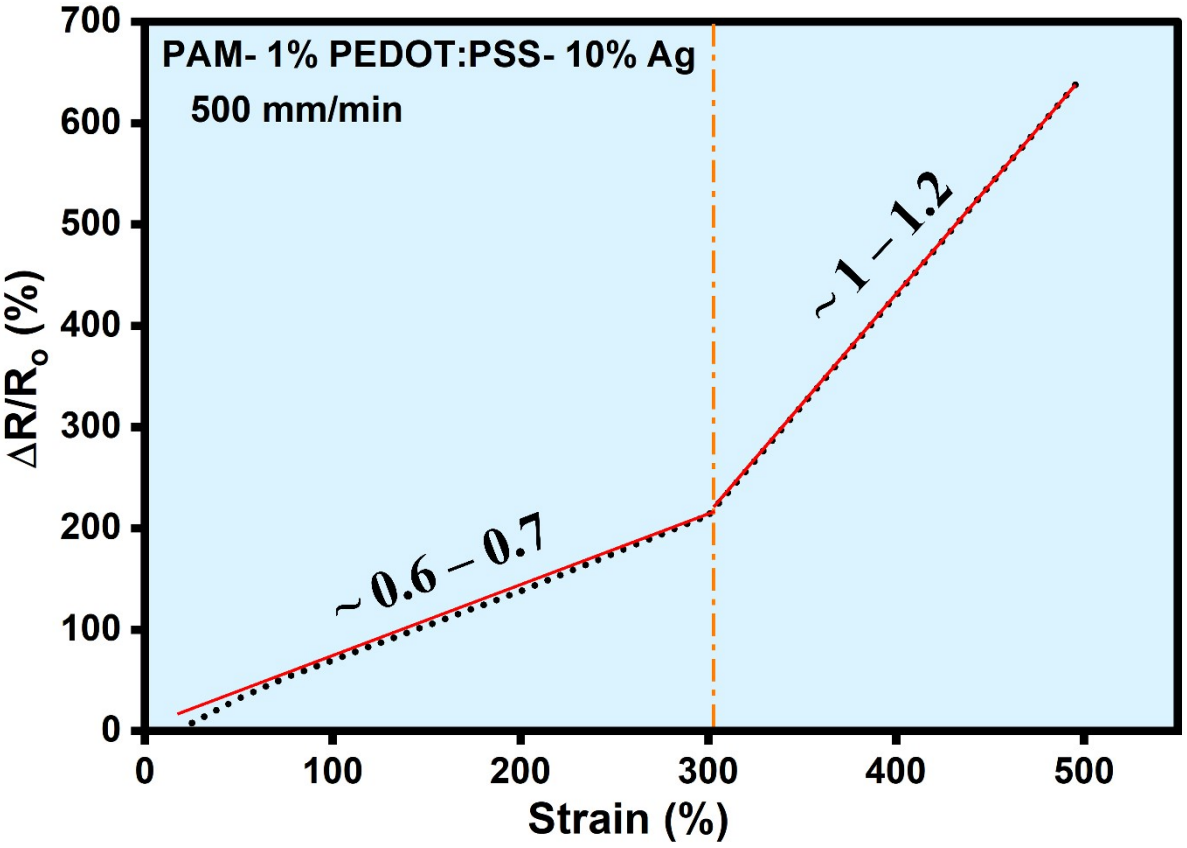

Supporting Figure 10: Gauge factors and relative resistance changes ($\Delta R/R_o$ %) in PAM-1% PEDOT: PSS- 10% Ag hydrogel at 25 to 500% strains at a 500 mm/min rate.

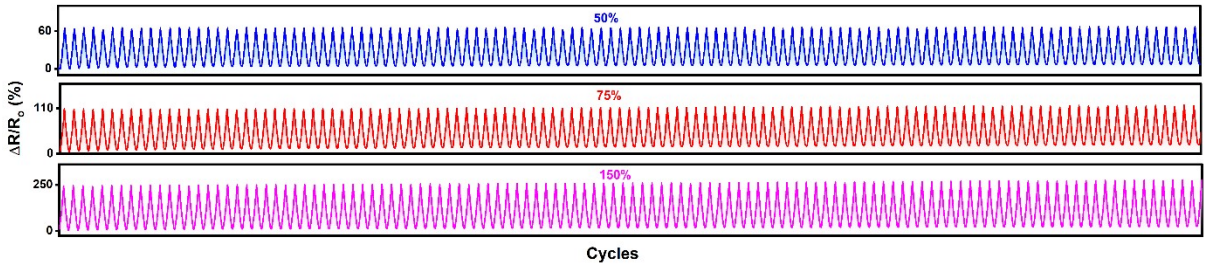

Supporting Figure 11: 100 repeated stretching/releasing cycles of PAM-1% PEDOT: PSS-10% Ag hydrogel at 50%, 75%, 150% strain.

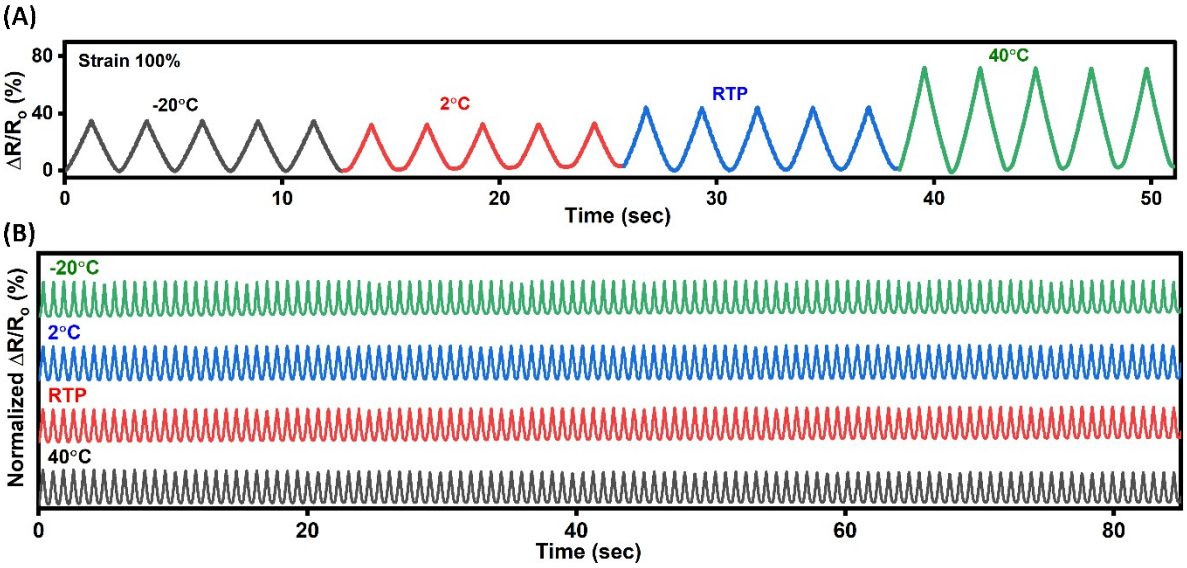

Supporting Figure 12: Temperature-dependent strain sensing and multifunctional performance of the PAM-1% PEDOT: PSS-10% Ag hydrogel. (A) Relative resistance change ($\Delta R/R_o$) under cyclic 100% strain at four temperatures: –20 °C, 2 °C, room temperature (RTP), and 40 °C, illustrating the nonmonotonic electromechanical response due to temperature-dependent network mechanics, ionic transport, and plasmonic hot-electron activity. (B) Stability of normalized $\Delta R/R_o$ over 100 strain cycles at the same temperature conditions, confirming consistent performance and durability across thermal environments.

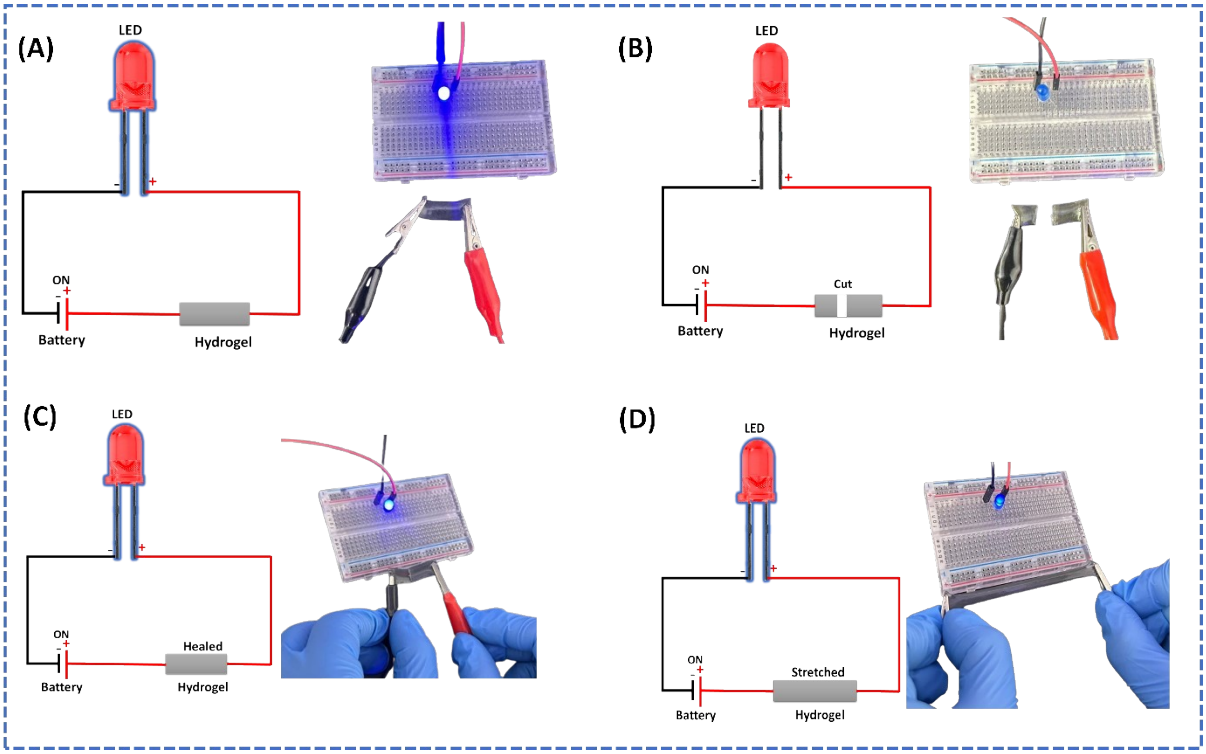

Supporting Figure 13: Visual demonstration of PAM-1% PEDOT: PSS- 10% Ag hydrogel functionality in an LED circuit. (A) Intact PAM-1% PEDOT: PSS- 10% Ag hydrogel completes the circuit, lighting the LED. (B) The PAM-1% PEDOT: PSS- 10% Ag hydrogel is cut, breaking the circuit, and turning off the LED. (C) PAM-1% PEDOT: PSS- 10% Ag hydrogel self-heals, restoring conductivity and reactivating the LED. (D) PAM-1% PEDOT: PSS- 10% Ag hydrogel is stretched, maintaining conductivity and LED illumination, confirming its mechanical resilience and suitability for dynamic bioelectronic applications

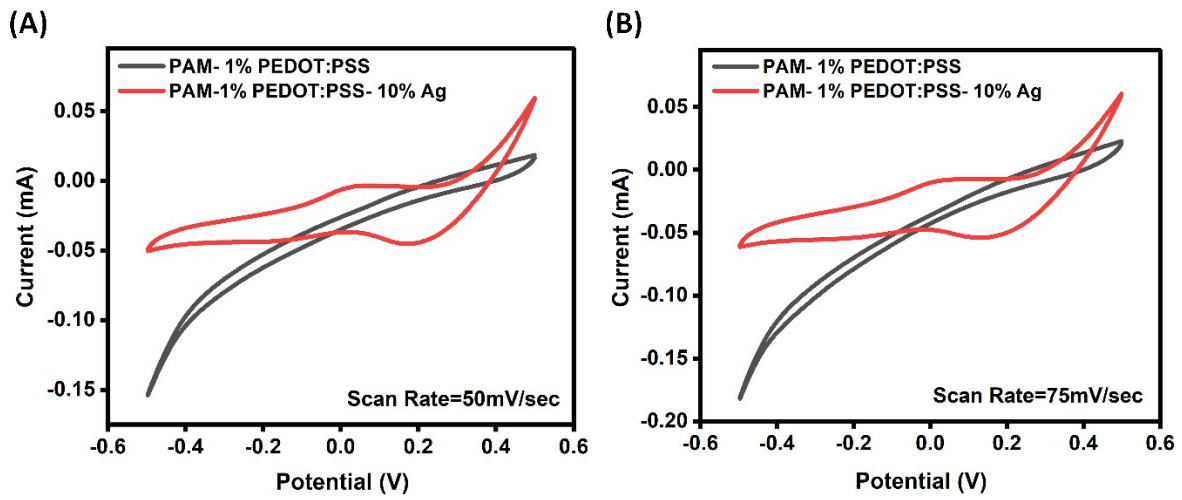

Supporting Figure 14: Cyclic voltammograms (CVs) of PAM-1% PEDOT: PSS and PAM-1% PEDOT: PSS-Ag 10% hydrogel (A). Cyclic voltammograms (CVs) of PAM-1% PEDOT: PSS and PAM-1% PEDOT: PSS-10% Ag hydrogel at a scan rate of 50 mV/s. (B). Cyclic voltammogram (CVs) of PAM- 1% PEDOT: PSS and PAM-1% PEDOT: PSS- 10% Ag hydrogel at a scan rate of 75 mV/s.

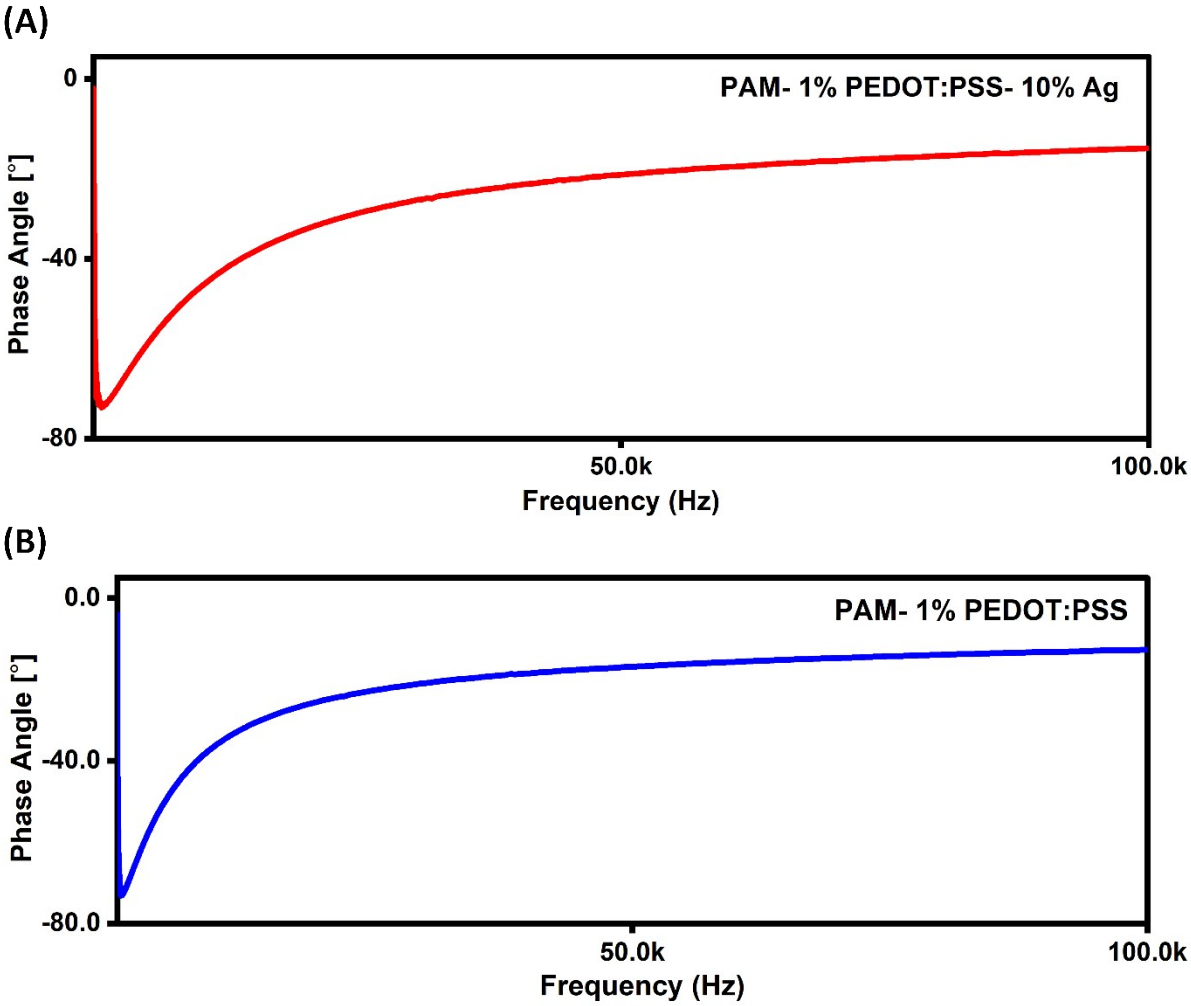

Supporting Figure 15: Electrode-skin electrochemical characterization. (A) Electrode skin phase angle measurement of PAM- 1% PEDOT: PSS-10% Ag hydrogel from 1Hz to 100K Hz. (B) Electrode skin phase angle measurement of PAM- 1% PEDOT: PSS- hydrogel from 1Hz to 100K Hz.

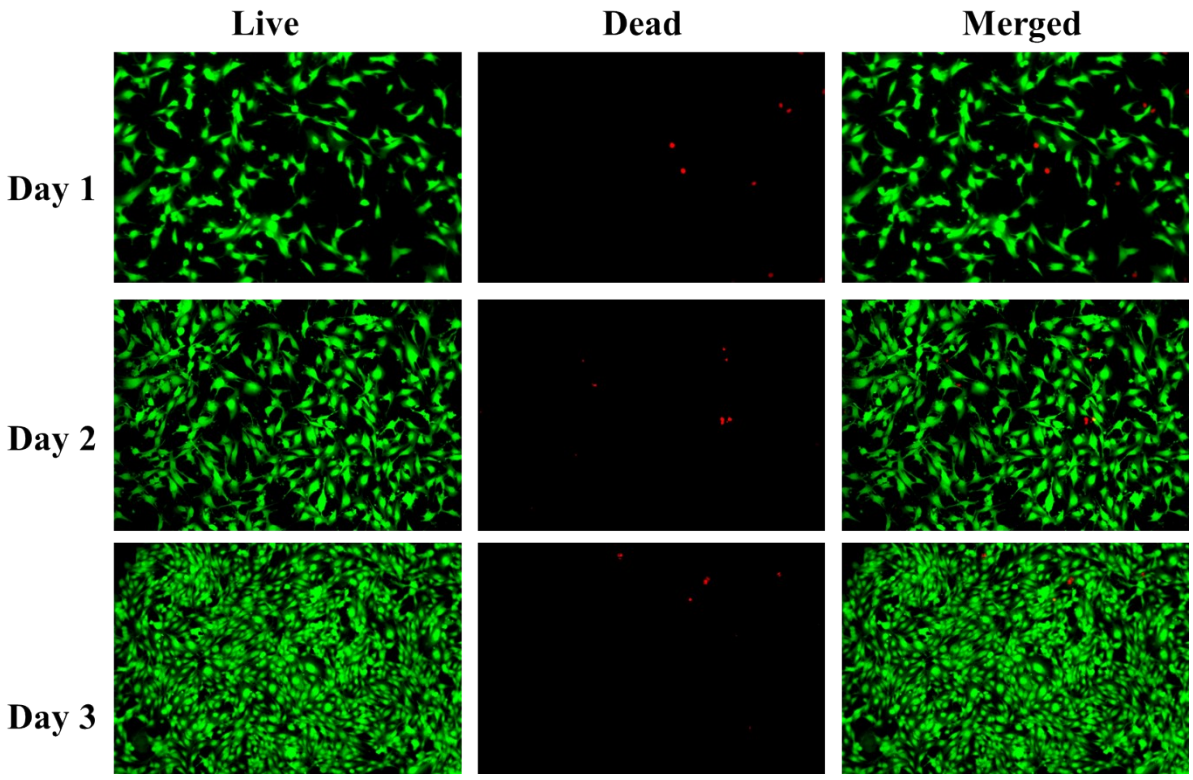

Supporting Figure 16: Fluorescence Cell Viability of Control over 3 days.

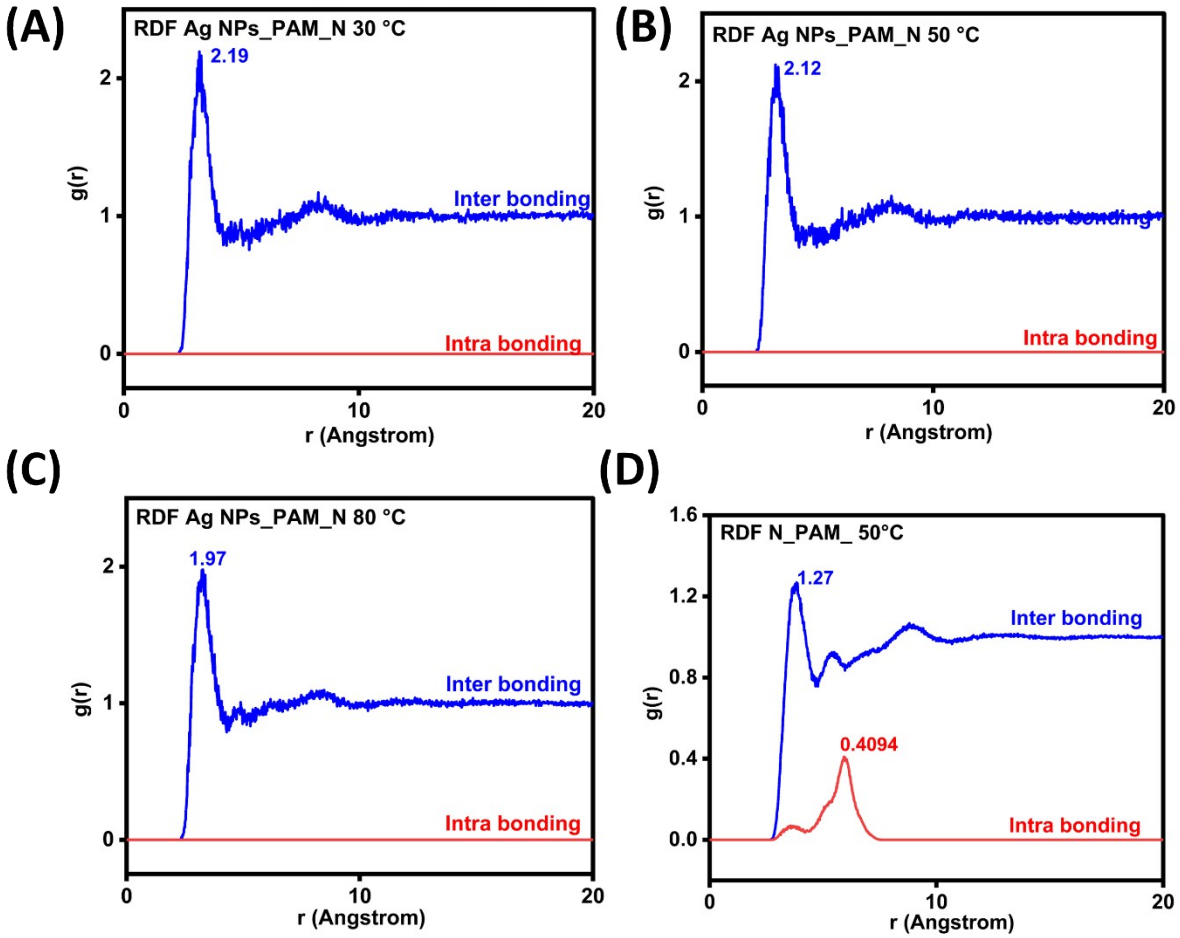

Supporting Figure 17:MD simulations of the PAM-PEDOT: PSS-Ag hydrogel system. (A) Radial Density Function (RDF) plot of Ag-NPs-PAM_N at 30 °C, (B) Radial Density Function (RDF) plot of Ag-NPs-PAM_N at 50 °C, (C) Radial Density Function (RDF) plot of Ag-NPs-PAM_N at 80 °C, (D) Radial Density Function (RDF) plot of PAM_N at 50 °C,

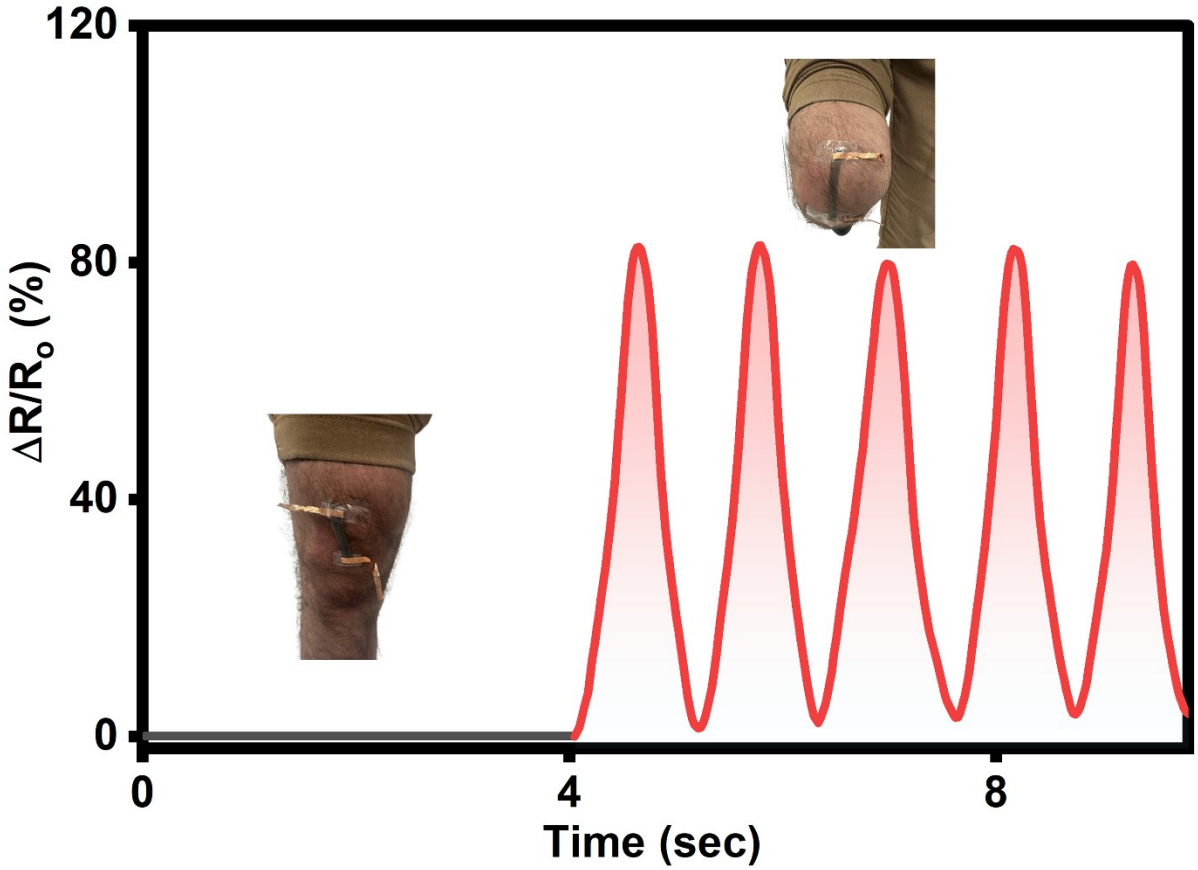

Supporting Figure 18: Real-time monitoring of relative resistance changes ($\Delta R/R_0$) during patellar region bending.

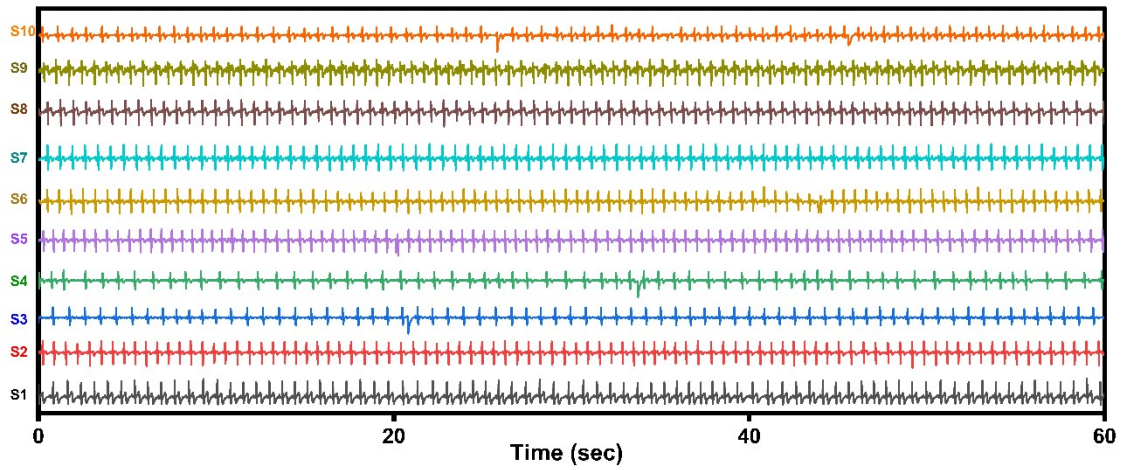

Supporting Figure 19: ECG data from 1-10 subjects were used for model training and testing.

References:

[1] X. Xiong, Y. Chen, Z. Wang, H. Liu, M. Le, C. Lin, G. Wu, L. Wang, X. Shi, Y.-G. Jia,

Polymerizable rotaxane hydrogels for three-dimensional printing fabrication of wearable sensors, Nature communications 14(1) (2023) 1331.
[2] Y. Zhao, Y. Ohm, J. Liao, Y. Luo, H.-Y. Cheng, P. Won, P. Roberts, M.R. Carneiro, M.F. Islam, J.H. Ahn, A self-healing electrically conductive organogel composite, Nature Electronics 6(3) (2023) 206-215.
[3] Q. Rong, W. Lei, L. Chen, Y. Yin, J. Zhou, M. Liu, Anti-freezing, conductive self-healing organohydrogels with stable strain-sensitivity at subzero temperatures, Angewandte Chemie International Edition 56(45) (2017) 14159-14163.
[4] X. Li, L. He, Y. Li, M. Chao, M. Li, P. Wan, L. Zhang, Healable, degradable, and conductive MXene nanocomposite hydrogel for multifunctional epidermal sensors, Acs Nano 15(4) (2021) 7765-7773.
[5] T. Chu, Y. Xiao, H. Lai, L. Shi, Y. Cheng, J. Sun, Z. Pang, S. Cheng, K. Zhao, Z. Gao, Highly Conductive, Adhesive and Biocompatible Hydrogel for Closed-Loop Neuromodulation in Nerve Regeneration, ACS nano 19(19) (2025) 18729-18746.
[6] Q. Liang, Z. Shen, X. Sun, D. Yu, K. Liu, S.M. Mugo, W. Chen, D. Wang, Q. Zhang, Electron conductive and transparent hydrogels for recording brain neural signals and neuromodulation, Advanced Materials 35(9) (2023) 2211159.
[7] J. Liao, Z. Ma, S. Liu, W. Li, X. Yang, M.E. Hilal, X. Zhou, Z. Yang, B.L. Khoo, Programmable Microfluidic-Assisted Highly Conductive Hydrogel Patches for Customizable Soft Electronics, Advanced Functional Materials 34(41) (2024) 2401930.
[8] X. Zhang, Y. Su, J. Xu, Y. Jin, H. Zhang, G. Ma, J. Xu, M. Zhou, X. Zhou, F. Cao, Self-Adhesive ILn@ MXene multifunctional hydrogel with excellent dispersibility for human-machine interaction, capacitor, antibacterial and detecting various physiological electrical signals in humans and animals, Nano Energy 133 (2025) 110484.
[9] M. Zhao, T. Wu, X. Wang, L. Liang, S. Zhang, T. Yuan, G. Fang, Exploration of hydroxyethyl cellulose-templated PEDOT: PSS for the development of high-performance conductive dual-network hydrogel strain sensor, Chemical Engineering Journal (2025) 165000.
[10] S. Soni, R. Wadhwa, M. Rishi, J. Kalra, A. Teja, D.D. Bhatia, D. Gupta, High-Performance Polyacrylamide Hydrogel-Based Wearable Sensors for Electrocardiography Monitoring and Motion Sensing, ACS Applied Electronic Materials 7(9) (2025) 4025-4034.
[11] X. Shi, L. Xu, Q. Xu, N. Li, X. Li, Y. Zhang, Z. Qin, T. Jiao, Ultrasoft Conducting Polymer Hydrogels with Large Biaxial Strain and Conformal Adhesion for Sensitive Flexible Sensors, Chemistry of Materials 36(21) (2024) 10560-10570.
[12] D. Bi, N. Qu, W. Sheng, T. Lin, S. Huang, L. Wang, R. Li, Tough and strain-sensitive organohydrogels based on MXene and PEDOT/PSS and their effects on mechanical properties and strain-sensing performance, ACS Applied Materials & Interfaces 16(9) (2024) 11914-11929.
[13] W. Zhang, X. Zhang, W. Zhao, X. Wang, High-sensitivity composite dual-network hydrogel strain sensor and its application in intelligent recognition and motion monitoring, ACS Applied Polymer Materials 5(4) (2023) 2628-2638.
[14] L. Lin, X. Jing, G. Wang, J. Yang, Y. Zhang, J. Zeng, C. Zhang, X. Liu, Fabrication of high-toughness, puncture-resistant hydrogels based on nanoengineered MXene for flexible electronics, ACS Applied Polymer Materials 6(18) (2024) 11497-11507.
[15] L. Xu, S. Liu, L. Zhu, Y. Liu, N. Li, X. Shi, T. Jiao, Z. Qin, Hydroxypropyl methyl cellulose reinforced conducting polymer hydrogels with ultra-stretchability and low hysteresis as highly sensitive strain sensors for wearable health monitoring, International Journal of Biological Macromolecules 236 (2023) 123956.
[16] H. Yin, L. Chen, F. Liu, T. Abdiryim, J. Chen, X. Jing, Y. Li, M. Su, X. Liu, MXene-based conductive hydrogels with toughness and self-healing enhancement by metal coordination for flexible electronic devices, Materials Today Physics 47 (2024) 101537.
[17] Y. Feng, H. Liu, W. Zhu, L. Guan, X. Yang, A.V. Zvyagin, Y. Zhao, C. Shen, B. Yang, Q. Lin, Muscle-inspired MXene conductive hydrogels with anisotropy and low-temperature tolerance for wearable flexible sensors and arrays, Advanced Functional Materials 31(46) (2021) 2105264.
[18] H. Liao, X. Guo, P. Wan, G. Yu, Conductive MXene nanocomposite organohydrogel for flexible, healable, low-temperature tolerant strain sensors, Advanced Functional Materials 29(39) (2019) 1904507.
[19] Y. Wei, L. Xiang, H. Ou, F. Li, Y. Zhang, Y. Qian, L. Hao, J. Diao, M. Zhang, P. Zhu,

MXene-based conductive organohydrogels with long-term environmental stability and multifunctionality, Advanced Functional Materials 30(48) (2020) 2005135.
[20] S.-N. Li, Z.-R. Yu, B.-F. Guo, K.-Y. Guo, Y. Li, L.-X. Gong, L. Zhao, J. Bae, L.-C. Tang, Environmentally stable, mechanically flexible, self-adhesive, and electrically conductive Ti3C2TX MXene hydrogels for wide-temperature strain sensing, Nano Energy 90 (2021) 106502.